IEEE Access
Multidisciplinary | Rapid Review | Open Access Journal

Received September 12, 2020, accepted September 30, 2020, date of publication October 15, 2020,
date of current version October 30, 2020.

Digital Object Identifier 10.1109/ACCESS.2020.3031278

A Micro Piezoelectric Motor With Multiple Excitation Modes and Methods

CHONG LI[1] AND CUNYUE LU[2]
[1]College of Electronic and Electric Engineering, Henan Normal University, Xinxiang 453007, China
[2]Department of Instrument Science and Engineering, Shanghai Jiao Tong University, Shanghai 200240, China

Corresponding author: Chong Li (uestc2007@yeah.net)

This work was supported in part by the Aisheng Fund for Innovation and Development under Grant ASN-IF2015-1302, in part by the Henan Provincial Education Department Project under Grant 19A535002, and in part by the Henan Key Laboratory of Optoelectronic Sensing Integrated Application and Ph.D. Scientific Research Start-Up Subject under Grant 5101239170004.

ABSTRACT To widen the performance of piezoelectric motors, this paper demonstrates a micro piezoelectric motor having multiple driving ways. The stator includes a hollow polygon bar and two groups of PZT plates. PZT plates are symmetrically bonded onto a brass base, and used to actuate the vibration modes of the stator. The symmetrical design enables the motor to operate in two types of vibration modes. The working modes are the second/third-order in-plane bending modes, and can be excited by different ways. Elliptical motion of stator surface points is generated by superposition of two bending modes with the same order. To investigate the feasibility of multi-mode and multi-motivation mechanisms, vibration behaviors of stator driving particles are simulated using ANSYS software. The structural parameters of the stator are strictly designed to harmonize the eigenfrequencies of the vibration modes. The calculated results reveal that the motor performance can be adjusted by selecting different operating modes and excitation ways. The motor performances under various excitation ways and driving modes are also investigated experimentally to validate the proposed design. The dimension of the fabricated prototype motor is 8.3 mm × 7.2 mm × 15.0 mm. The maximum torques are respectively 8.3 cN·m and 13.3 cN·m under single-phase and two-phase excitation voltages, when the motor operates in the second-order bending modes. The corresponding no-load speeds are respectively 40 rpm and 47 rpm. The maximum torque and speed under the third-order bending modes are much smaller than that under the second-order bending modes.

INDEX TERMS Piezoelectric motor, bending modes, multi-motivation, ANSYS.

I. INTRODUCTION

In-vivo medical devices such as wireless capsules have unique advantages and already been commercially manufactured by leading companies [1]. However, lack of locomotion control element over these devices introduces low diagnostic yields and false positive results [1].

Piezoelectric motors are appropriate for miniaturization and show great potentials in in-vivo medical fields [2]–[6]. Nowadays, micro piezoelectric motors have been brought forward and widely used as direct-drive modules [7]–[15]. The most typical micro piezoelectric motor was proposed by Uchino. Owing to the asymmetrical stator structure, two degenerated orthogonal bending modes were slightly split [14]. A sinusoidal signal is used to yield micro mechanical vibrations of the stator by using the d_{31} effect of piezoelectric ceramics. Then, a wobbling motion of the composite stator is generated. Nevertheless, these piezoelectric motors are driven by out-of-plane bending modes [12]–[15]. The stator is developed with a slim and long configuration, which probably restricts its application in in-vivo [15]–[17]. To limit the height of piezoelectric motors, a compact motor operating in the d_{15} shear-mode was designed [15]. The motor has basically a flat and wide construction. The energy conversion rate from electrical to mechanical of this motor is much higher than that of the d_{31} type [15]. The bonded piezoelectric disc was poled along the radial direction. The bottom electrode of piezoelectric disc was divided into four parts with keeping the top electrode common [15]. However, the radially polarized piezoelectric disc is difficult to machine. The working modes of piezoelectric motors [7]–[15] are typically fixed, and cannot be electrically excited by

The associate editor coordinating the review of this manuscript and approving it for publication was Junxiu Liu.

multiple ways. It means that the motor performance is unable to be adjusted by excitation ways and vibration modes. Therefore, the piezoelectric motors are incapable of meeting different performance requirements simultaneously. To accurately predict disease information [18]–[20], the proposed piezoelectric motor should be able to offer a wider performance, and satisfy the demand for diverse rotation speeds and torques at different observation positions [21]–[24].

Aiming at larger performance flexibility with respect to different application needs, a micro piezoelectric motor driven by adjustable vibration modes and motivation patterns is presented. The motor operates in two second/third-order in-plane bending modes on the d_{33} effect of piezoelectric ceramics. The bending modes with the same order can be simultaneously actuated by multiple ways. The generated vibration characteristic of the motor varies considerably among different excitation methods, and can be chosen flexibly by applying actuation voltages on varied PZT plates. The motor performance can also be regulated by electing different operating modes. Accordingly, the designed motor can achieve sufficient performance by selective excitation of the second or third resonance vibration modes of the stator, or adopting different incentive ways. The adjustable incentives represent an appropriate approach to make motor performance more flexible. The use of d_{33} effect also helps to increase the piezoelectric motor's application capacity. Additionally, the in-plane vibration modes are useful for motor miniaturization. These features contribute to controlling the speed and torque of piezoelectric motor used in in-vivo medical devices.

II. STRUCTURE AND MODE EXCITATION PRINCIPLE

Fig. 1(a) shows a schematic illustration of the developed piezoelectric motor. It consists of a stator, a rotor, and a prepressure mechanism. The stator is indicated in Fig. 1(b). It is composed of a thin brass base and two groups of PZT plates, PZT-A and PZT-B. PZT-A_1 and PZT-A_2 constitute one group of PZT plates, PZT-A. PZT-B_1 and PZT-B_2 compose the other group of PZT plates, PZT-B. Among them, PZT-A_2 and PZT-B_2 are divided into two partitions as shown in Fig. 1(c). Four rectangular PZT plates are symmetrically attached to the brass base using epoxy resin adhesive [6]. The internal and external surfaces of PZT plates are covered with conductive electrodes. PZT plates are polarized along the thickness direction illustrated by the arrows in Fig. 1(c), and utilized to generate flexion vibrations of the stator. Then, elliptical movement of stator driving points is created. The rotor is pressed against the stator's surface. The preload between the stator and rotor is applied mechanically by a spring. Rotation is produced via frictional interaction between the contact surface of the stator and rotor.

The piezoelectric motor uses a combination of two bending modes for generation of rotor rotation. A single-phase driving way of the second-order bending modes has been briefly discussed [6]. In this paper, the improved motor possesses multiple excitation modes. Depending on the geometry of the

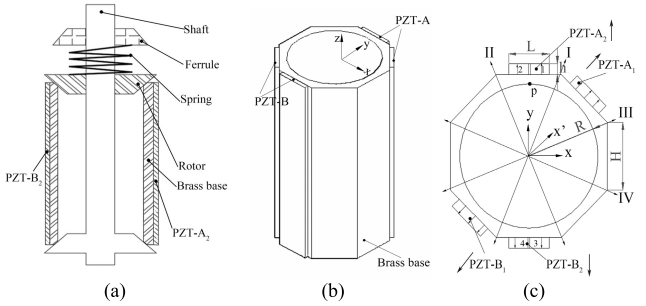

FIGURE 1. (a) The configuration of the motor; (b)The three-dimensional structure of the stator; (c) The parameters of the stator.

stator, it can operate in two kinds of vibration modes. The working modes are the second-order in-plane bending modes as shown in Fig. 2, or the third-order in-plane bending modes as indicated in Fig. 3. Moreover, these operating modes can be excited by multiple methods. All the excitation means will be specifically discussed in Section III.

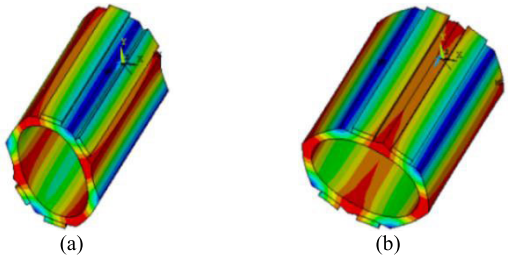

FIGURE 2. The second-order in-plane bending modes: (a) Mode A; (b) Mode B.

Fig. 2 indicates that PZT-A_i and PZT-B_i (i = 1/2) synchronously elongate/contract. Thus, there are more single-phase incentive ways. Besides, by applying two-phase voltages with a 90-degree phase difference to two/three/four PZT plates, the standing waves of the two bending modes can also be actuated. A travelling wave is generated around the circumference of stator through-hole by combining the second-order response modes. When four PZT plates are supplied with two-phase voltages, the performance of the motor operating in Modes A and B will be maximized. Under this condition, a sine voltage is applied to the outer surface electrodes of PZT-A_2 and PZT-B_2. A cosine voltage is supplied to the outer surface electrodes of the other PZT plates. The metal base is grounded. Consequently, the motor operating in the second-order in-plane bending modes has various driving schemes.

The excitation mechanism of the third-order bending modes is slightly different from that of the second-order bending modes. The applied actuation voltages should be arranged according to the displacement nephogram of the stator. Fig. 3 indicates that when PZT-A_i stretches, PZT-B_i contracts (i = 1/2). Consequently, the applied voltage of PZT-A_i and PZT-B_i (i = 1/2) should be reversed. Concretely, PZT-V_1 and PZT-V_2 are supplied with an alternating voltage

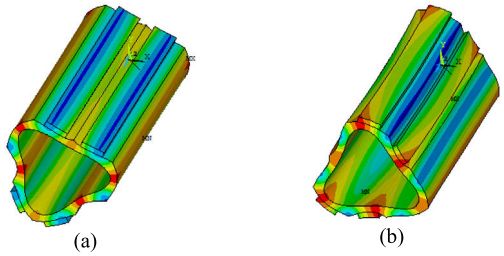

FIGURE 3. The third-order in-plane bending modes: (a) Mode C; (b) Mode D.

to excite Mode C. Meanwhile, PZT-V_2 (V = A/B) should be supplied with another alternating voltage to excite Mode D. These analyses illustrate that two-phase voltages should be used to simultaneously excite Modes C and D. Furthermore, by applying two-phase voltages to two/three/four PZT plates can all actuate the vibration modes. If two-phase voltages are applied to all PZT plates, the motor performance reaches its maximum value under Modes C and D.

Additional PZT plates can also be adhered to the rest surfaces of the brass base, on the basis of unchanging the stator's symmetry. The added PZT plates can be utilized to apply actuation voltages and excite the vibration modes. The excitation way of the working modes is further increased. The performance of the motor is also further broadened.

III. FINITE ELEMENT ANALYSIS

The behavior of the free stator is simulated using the finite element software ANSYS to theoretically verify multiple drive mechanism. To build the three-dimensional finite element model of the stator, PZT plates are meshed using the 3D coupled-field solid element SOLID5. The SOLID5 element has eight nodes with up to six degrees of freedom at each node. The brass base is modeled using the 3D solid element SOLID73 defined by eight nodes.

Modal analysis is carried out to tune the natural frequencies of the vibration modes. Table 1 lists the material properties

TABLE 1. The material properties of the stator.

Material	Brass base	PZT plates
Density (kg/m^3)	7500	8900
Elastic modulus (×10^{10} N/m^2)	$\begin{pmatrix} 13.9 & 7.78 & 7.43 & 0 & 0 & 0 \\ & 13.9 & 7.43 & 0 & 0 & 0 \\ & & 11.5 & 0 & 0 & 0 \\ & & & 2.56 & 0 & 0 \\ & & & & 3.06 & 0 \\ & & & & & 2.56 \end{pmatrix}$	11.7
Piezoelectric constant (C/m^2)	$\begin{pmatrix} 0 & 0 & -1.23 \\ 0 & 0 & -1.23 \\ 0 & 0 & 2.89 \\ 0 & 4.96 & 0 \\ 4.96 & 0 & 0 \\ 0 & 0 & 0 \end{pmatrix}$	

of the stator structural model. The thickness of PZT plates h, the inner radius of brass base R, the side length of octagon H, and the length of PZT plates L, as shown in Fig. 1(c), are chosen to regulate the resonance frequencies of the vibration modes. These structural parameters are strictly designed to harmonize the eigenfrequencies of two second/third-order in-plane bending modes, and then achieve multiple excitation ways under two types of operating modes. When the resonance frequencies of two vibration modes of the same order are nearly identical, the superposition of them will happen under specific voltage excitation source. Then, a superimposed travelling wave is generated in the stator. The simulation results signify that the resonance frequencies of the vibration modes are independent of the height of motor. Hence, the height can be further reduced. The optimal structural parameter values of R, H, h, and L are respectively 3 mm, 3 mm, 0.5 mm and 2.5 mm. These parameter values are different from the ones reported in preceding paper [6], because the resonance frequencies of the second/third-order bending modes should both be harmonized. Table 2 gives the calculated resonance frequencies of the bending modes under zero voltage boundary conditions and free-free mechanical boundary conditions.

TABLE 2. The resonance frequencies of the operating modes.

Mode	A	B	C	D
f (kHz)	16.84	17.18	47.32	47.28

Harmonic analysis is subsequently conducted to investigate the displacement characteristic of the stator in frequency domain. The vibration characteristics of the stator excited by single-phase voltage are firstly analyzed. All feasible single-phase incentive ways of the second-order bending modes are given in Table 3. Each cell of Table 3 represents a single-phase actuation way. In each cell, a sine voltage is applied on the listed PZT plates. The other PZT plates are floating. The brass base is grounded. The response displacement of each column is the same under corresponding single-phase excitation ways. The peak amplitude of input voltage is 45 V. The sub-step is twenty. Table 3 reports the obtained maximum amplitudes of U_x, U_y and U_z of the driving point p that is shown in Fig. 1(c). The resonance frequencies of Modes A and B under harmonic analysis are also given in Table 3. These results imply that the resonance frequencies of Modes A and B under different single-phase excitation ways are slightly varied. Additionally, not all single-phase incentive methods can simultaneously actuate the operating modes. The single-phase voltage applied to PZT-V_1 and PZT-V_2 (V = A/B) results in Mode A not to be excited. The reason is that superposition of excited vibrations in the y and x' directions of the stator leads to a vibration along the I direction. Whereas, the vibration along the IV direction is offset.

The vibration characteristics of the stator driven by two-phase voltages are also compared. Specifically, the brass base

TABLE 3. The maximum displacements of the driving point p and resonance frequencies of the second-order bending modes under single-phase voltage.

U/f (μm/kHz)	Applying single-phase excitation voltage on listed PZT plates		
	PZT-A_1 PZT-A_2 PZT-B_1 PZT-B_2	PZT-A_1 and PZT-B_1 **PZT-A_2 and PZT-B_2**	PZT-A and PZT-B_1 PZT-A and PZT-B_2 PZT-B and PZT-A_1 PZT-B and PZT-A_2
U_x/f	2.00/17.05	3.99/16.90	2.03/16.85
U_y/f	2.53/17.60	5.07/17.55	7.68/17.30
U_z/f	0.05/17.05	0.10/16.90	0.15/16.85

is grounded. Two-phase voltages with the maximum value of 45 V and phase difference of 90-degree are applied on selected PZT plates. Table 4 summarizes two-phase excitation ways of the second-order bending modes. Each column of Table 4 displays a two-phase actuation way. V_1 and V_2 represent two-phase input voltages. Table 4 also gives the calculated maximum amplitudes of U_x, U_y, and U_z of the driving point. The resonance frequencies of the second-order operating modes are also included in Table 4. The simulation results reveal that all the listed two-phase excitation patterns can simultaneously excite the second-order bending modes. It can also be observed from the results in Table 4 that applying two-phase excitation voltages on arbitrary two/three/four PZT plates can all actuate the second-order operating modes. Thus, there still are some feasible two-phase excitation ways that is not given in the table.

Table 5 shows two-phase excitation methods of the third-order bending modes. Each column of Table 5 represents a two-phase actuation way. The numbers in brackets indicate different partitions of PZT-A_2 and PZT-B_2. Table 5 also exhibits that all the two-phase excitation ways can stimulate the third-order bending modes. Besides, applying two-phase voltages on arbitrary two/three/four PZT plates can all excite the third-order bending modes. The maximum displacement of the driving point in Table 5 is smaller than that in Table 4. It means that compared with high-order vibration modes, response displacements of stator surface points driven by low-order modes are larger under the same exciting voltage.

As can be seen from Tables 2-5, a slight variation in the resonance frequencies of the operating modes is observed between modal and harmonic response analyses. The difference is mainly caused by the amplitude of applied voltage in harmonic analysis. The number of sub-steps also affects the accuracy of computed resonance frequency. Tables 3-5 show that the displacement amplitudes of U_x and U_y are more than ten times larger than that of U_z. It verifies that the stator mainly vibrates in x-y plane.

To further investigate motion behaviors of particles on the stator surface in time domain, transient analysis is performed. The above analysis implies that there are many ways to stimulate the operating modes. For simplicity, three typical driving methods bolded in Tables 3-5 are analyzed. The structural loss is considered by applying Rayleigh damping [22]–[24]. Firstly, an alternating voltage with the maximum amplitude of 45 V and frequency of 17.30 kHz is applied to PZT-A_2 and PZT-B_2. The excitation voltage is discretized by 40 data points per cycle. The displacement-time curve of the driving point under single-phase voltage is shown in Fig. 4. Due to the existence of Rayleigh damping, the vibration displacements are smaller than the results achieved from harmonic response analysis.

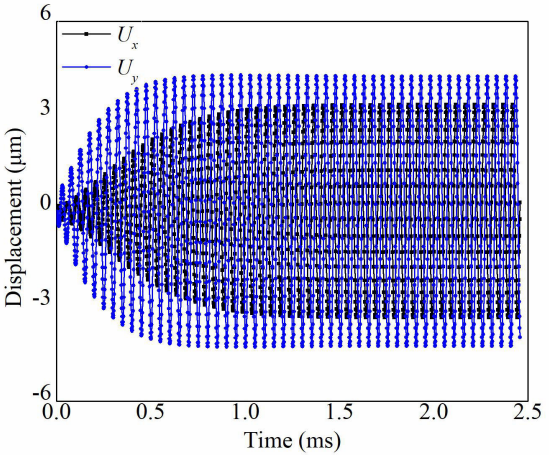

FIGURE 4. Numerical simulation results of vibration displacements in time domain.

Fig. 5 presents the motion trajectory of the driving point under single-phase voltage. It illustrates that the stator moves with elliptical trace, and the proposed motor can operate in single-phase voltage. The vibration displacement and resultant trajectory can be adjusted by altering the exciting frequency, or choosing different single-phase excitation ways. These results theoretically confirm the feasibility of the single-phase driving mechanism for the designed piezoelectric motor operating in Modes A and B.

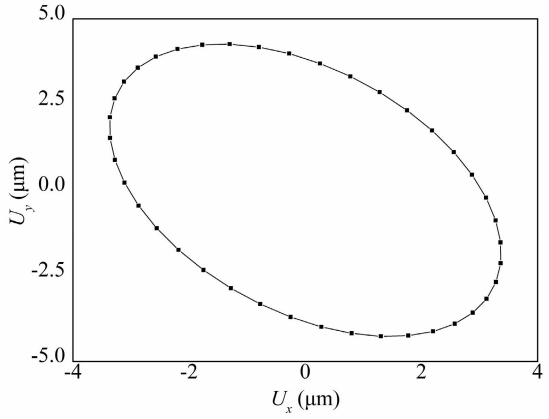

FIGURE 5. Elliptical trajectory of the driving point p on the stator surface.

Secondly, the vibration displacements of the driving point in response to two-phase voltages are also calculated. Two-phase alternating voltages of frequency 17.00 kHz are respectively applied to all PZT plates to excite Modes A and B.

TABLE 4. The maximum displacements of the driving point p and resonance frequencies of the second-order bending modes under two-phase voltages.

Voltage	Applying two-phase excitation voltages on selected PZT plates								
$V\cos\omega t$	PZT-A_1	PZT-A_2	PZT-A_1	PZT-B_1	PZT-A_1	PZT-A_2	PZT-A_1 and PZT-B_1	PZT-A_1 and PZT-B_1	**PZT-A_1 and PZT-B_1**
$V\sin\omega t$	PZT-B_1	PZT-B_2	PZT-A_2	PZT-B_2	PZT-B_2	PZT-B_1	PZT-A_2	PZT-B_2	**PZT-A_2 and PZT-B_2**
U_x/f	2.34/16.90	2.34/16.90	3.13/17.00	3.13/17.00	3.05/17.00	3.05/17.00	4.64/17.00	4.64/17.00	6.29/16.79
U_y/f	2.40/17.55	2.40/17.55	3.86/17.45	3.86/17.45	3.97/17.40	3.97/17.40	2.68/17.36	2.68/17.36	7.75/17.12
U_z/f	0.04/16.90	0.04/16.90	0.09/17.00	0.09/17.00	0.09/17.00	0.09/17.00	0.07/17.00	0.07/17.00	0.16/17.09

TABLE 5. The maximum displacements of the driving point p and resonance frequencies of the third-order bending modes under two-phase voltages.

Voltage	Applying two-phase voltages on listed PZT plates			
$V\cos\omega t$	PZT-A_1 and half PZT-A_2 (2)	half PZT-A_2 (2), and PZT-A_1	half PZT-A_2 (2), and PZT-B_1	**half PZT-A_2 (2), and PZT-A_1**
$V\sin\omega t$	half PZT-A_2 (1)	half PZT-A_2 (1)	half PZT-A_2 (1)	**half PZT-A_2 (1)**
$-V\cos\omega t$		half PZT-B_2 (4)	PZT-A_1	**half PZT-B_2 (4) and PZT-B_1**
$-V\sin\omega t$		half PZT-B_2 (3)		**half PZT-B_2 (3)**
U_x/f	0.61/46.95	1.03/46.95	1.23/46.95	1.20/46.92
U_y/f	2.40/46.92	1.46/46.90	1.16/46.90	1.69/46.88
U_z/f	0.09/46.74	0.09/46.78	0.09/46.78	0.18/46.78

The phase difference between the exciting voltages is set to be 90-degree. The amplitude of two-phase voltages is 45 V. The stable displacement-time curve of the driving point under two-phase voltages is described in Fig. 6. The overall displacement-time characteristic of the driving point is in accordance with Fig. 4. There exists a phase difference between the response displacement U_x and U_y. The phase difference between U_x and U_y is about 45-degree. The vibration trajectory of the driving point under two-phase alternating voltages is also elliptical. These results theoretically confirm the feasibility of the two-phase driving principle for the piezoelectric motor. The vibration displacement and motion track can be further adjusted by changing the frequency or phase difference of two-phase actuation voltages, or choosing different two-phase excitation ways.

These simulation results demonstrate that the second-order bending modes can be driven by multiple ways. The response displacement is closely related to incentive pattern. The performance of the motor can be adjusted by adopting different incentives. According to Tables 3 and 4, there are at least eight different vibration characteristics.

Finally, the vibration displacements of the motor operating in the third-order bending modes in response to two-phase voltages are also calculated. The increasing trend of vibration displacement stimulated by the third-order modes is in conformity to Fig. 4. The superimposed vibration trajectory is elliptical. The vibration displacement and motion track can be adjusted by altering the frequency or phase difference of actuation voltages, or selecting different two-phase excitation ways. The transient analysis results further validate that the third-order bending modes can be excited by the listed two-phase excitation ways in Table 5. Four different vibration characteristics can be generated, when the motor operates in the third-order bending modes.

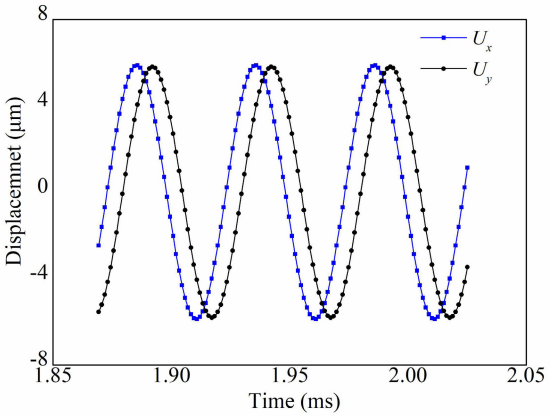

FIGURE 6. Stable displacements under two-phase excitation voltages.

IV. EXPERIMENTAL EVALUATION OF THE MICRO PIEZOELECTRIC MOTOR

Experimental studies are conducted to estimate the dynamic performance of the designed motor. The micro vibration displacements of stator driving points significantly influence the performance of piezoelectric motors. A scanning Laser Doppler Vibrometer (PSV-400-M2, Polytec GmbH, Waldbronn, Germany) is used to measure the vibration characteristic of the fabricated stator. The required experimental setup is shown in Fig. 7. The prototype motor stator in the test system is enlarged locally. The resonance frequencies of the bending modes can be derived by measuring the vibration characteristic of the stator under free-free boundary conditions. To simultaneously excite Modes A and B, a function generator and a power amplifier are used to provide single-phase driving voltage. In a frequency range from 15 kHz to 18 kHz, the continuous vibration response is scanned to find the resonance frequencies of the operating modes. By exciting

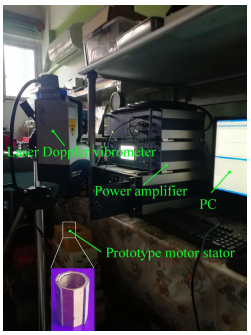

FIGURE 7. Test assembly of the piezoelectric motor.

PZT-A_2 and PZT-B_2, the vibration velocity along the I and II directions as shown in Fig. 1(c), is measured.

When the direction of incident laser is along the I direction, the vibration velocity response values of the two modes are approximately the same. The measured vibration velocity response spectrum is shown in Fig. 8(a). When the direction of incident laser is along the II direction, the vibration velocity response value of Mode A is larger than that of Mode B. The acquired vibration velocity response spectrum is illustrated in Fig. 8(b). It can be concluded from Fig. 8 that the resonance frequency of Mode A is 16.00 kHz. The resonance frequency of Mode B is 16.57 kHz. The resonant frequencies of Modes A and B under two-phase voltages are approximately the same as those under single-phase voltage. Fig. 8(a) also reveals that the resonance frequency of one of the third-order bending modes is about 46 kHz, according to the described excitation principle of the third-order bending modes.

The resonance frequencies of the third-order bending modes are also tested. PZT plates are supplied with two-phase voltage as described in Section II to excite Modes C and D. The measured the resonance frequencies of the third-order bending modes are 46.07 kHz and 46.65 kHz. The experimental resonance frequencies are slightly different from the theoretical values. This is mainly due to the bonding layer which is not considered in simulation, and machining errors. The epoxy layer between PZT plates and brass base affects the mechanical quality factor of the stator. This results in an inconsistence in the calculated and measured resonance frequencies of the presented motor.

A micro driver as shown in Fig. 9(a) is used to provide driving voltages, and measure the mechanical characteristic of the prototype motor. The generated two-phase square wave excitation voltage is shown in Fig. 9(b). Three typical incentive methods bolded in Tables 3-5 are performed in experiments as in transient analysis. An alternating voltage supplied by the micro driver is applied on PZT-A_2 and PZT-B_2 to excite the second-order bending modes under single-phase excitation. Whereas, two alternating voltages are applied on all PZT plates for two-phase excitation experiments. The phase difference of the two alternating voltages is 90-degree. The amplitude, frequency, and phase difference of the driving voltage can be adjusted by the micro driver.

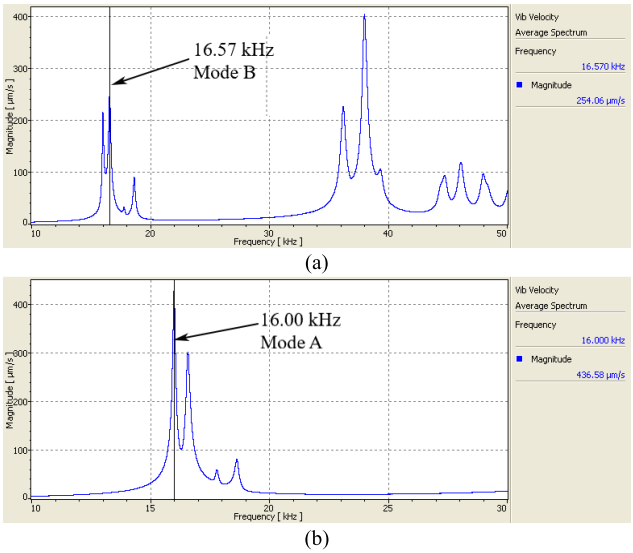

FIGURE 8. Vibration scan results of the prototype motor under single-phase voltage.

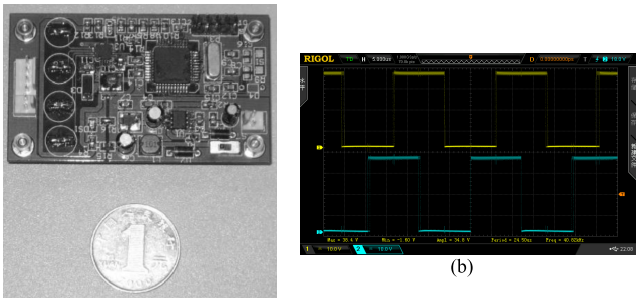

FIGURE 9. (a) The micro driver; (b) The generated two-phase drive voltage.

Fig. 10 displays the dependence of the motor's rotational speed on driving frequency. The amplitude of actuation voltage is set to be 45 V. The applied preload is 5 N. The preload is orthogonally applied to the stator by tightening the coil springs. The speed is estimated with a revolution counter. The data in Fig. 10 suggests that the prototype motor achieves a maximum rotary speed of 40 rpm under single-phase voltage, as the exciting frequency reaches 16.40 kHz. A maximum velocity of 47 rpm is attained under two-phase excitation voltages. The corresponding exciting frequency is 15.80 kHz. There is a slight deviation in frequencies corresponding to the maximum speed under the two incentive ways. The reason is that under single-phase actuation there is no voltage applied to PZT-A_1 and PZT-B_1. The floating PZT plate influences the vibrations of the stator and resonance frequencies of the second-order bending modes. It also means that the impedance characteristic of the stator is varied under different electrical boundary conditions. The maximum no-load speed reaches 9 rpm under the third order bending modes, which is smaller than that under the second-order bending modes.

Fig. 11 gives the load characteristics of the investigated motor. The torque is measured by pulling up the weight.

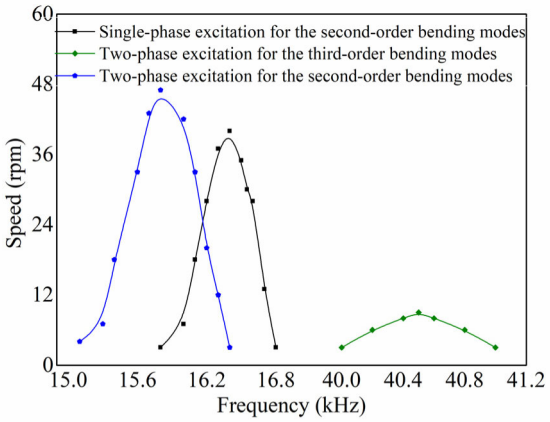

FIGURE 10. No-load speed characteristics.

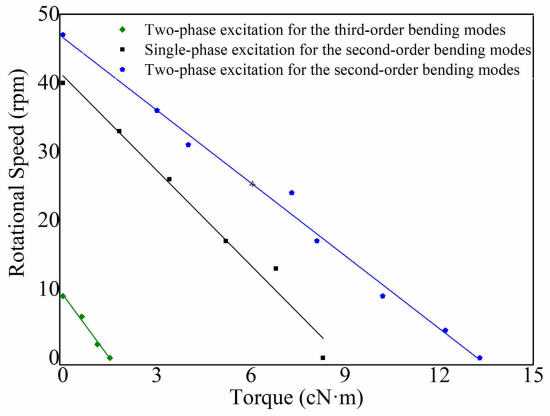

FIGURE 11. Plot of the speed versus the torque.

A best fitting curve is drawn joining the experimental results. The prototype motor respectively gains a maximum torque of 8.3 cN·m and 13.3 cN·m under single-phase and two-phase excitation voltages, when operating in Modes A and B. The maximum torque under Modes C and D is smaller than that under Modes A and B. The measurement results verify the effectiveness of the proposed multiple excitation methods. In addition, this motor possesses a significant performance advantage. It exhibits different performances under variable excitation ways and vibration modes. A suitable motivation approach can be chosen freely according to actual application needs.

V. CONCLUSION

A piezoelectric motor with adjustable output performances is presented. The motor is designed to satisfy different application requirements by choosing appropriate excitation ways and working modes. The stator comprises a metallic cube with a side length of 3 mm and a through-hole of 3 mm radius at its center, and four PZT plates. The exciting principle of the operating modes is analyzed. Elliptical motion of stator surface points is generated by superposition of two in-plane bending modes with the same order. The vibration features of the motor under various driving ways and vibration modes are simulated and compared by the finite element software ANSYS.

To validate the feasibility of the motor experimentally, a prototype motor is manufactured, and a set of experimental system is established. The size of the fabricated motor is 8.3 mm×7.2 mm×15.0 mm. The prototype motor driven by Modes A and B respectively gains a maximum torque of 8.3 cN·m and 13.3 cN·m under single-phase and two-phase excitation voltages. The corresponding no-load speeds are respectively 40 rpm and 47 rpm. The maximum torque and speed under Modes C and D are both much smaller than that under Modes A and B. Compared with prior piezoelectric motors [15]–[21], this motor can be flaky shape, and driven by a miniaturized circuit. The most significant difference between this design and the former ones is that the motor possesses different performances under variable excitation ways and vibration modes, and then has wider applicability. The designed motor yields significant improvements in terms of mode excitation mechanism, which is beneficial to broaden the motor performances. These features make the proposed motor to be beneficial to integrate into wireless capsules.

REFERENCES

[1] X. Ye, J.-J. Cabibihan, and W. J. Yoon, "Design and verification of a flexible device for steering a tethered capsule endoscope in the stomach," in *Proc. 14th Int. Conf. Ubiquitous Robots Ambient Intell. (URAI)*, Jeju, South Korea, Jun. 2017, pp. 550–555.

[2] Y. Shi and C. Zhao, "A new standing-wave-type linear ultrasonic motor based on in-plane modes," *Ultrasonics*, vol. 51, no. 4, pp. 397–404, May 2011, doi: 10.1016/j.ultras.2010.11.006.

[3] L.-K. Chang and M.-C. Tsai, "Design of single-phase driven screw-thread-type ultrasonic motor," *Rev. Sci. Instrum.*, vol. 87, no. 5, pp. 055002.1–055002.6 May 2016, doi: 10.1063/1.4948290.

[4] Z. Z. Chen, Y. Chen, and T. Y. Zhou, "A nut-type ultrasonic motor driven with single phase signal," *Vib. Eng. Technol. Machinery*, vol. 23, pp. 835–843, Aug. 2015, doi: 10.1007/978-3-319-09918-7_74.

[5] S.-T. Ho and S.-J. Jan, "A piezoelectric motor for precision positioning applications," *Precis. Eng.*, vol. 43, pp. 285–293, Jan. 2016, doi: 10.1016/j.precisioneng.2015.08.007.

[6] C.-Y. Lu, C. Li, and Y.-X. Ma, "A piezoelectric motor driven by a single-phase signal," *J. Vibroengineering*, vol. 19, no. 4, pp. 2645–2653, Jun. 2017, doi: 10.21595/jve.2016.17852.

[7] K. Yokoyama, "Single-phase drive ultrasonic linear motor using a linked twin square plate vibrator," *Jpn. J. Appl. Phys.*, vol. 33, pp. 461–462, Nov. 2012, doi: 10.7567/JJAP.52.07HE03.

[8] S.-W. Hsiao and M.-C. Tsai, "Single-phase drive linear ultrasonic motor with perpendicular electrode vibrator," *Jpn. J. Appl. Phys.*, vol. 49, no. 2, pp. 024201.1–024201.7, Feb. 2010, doi: 10.1143/JJAP.49.024201.

[9] C. Li, C.-Y. Lu, Y.-X. Ma, S.-Y. Li, and W.-Q. Huang, "Design of an ultrasonic motor with multi-vibrators," *J. Zhejiang Univ.-Sci. A*, vol. 17, no. 9, pp. 724–732, Sep. 2016, doi: 10.1631/jzus.A1500316.

[10] S.-T. Ho and Y.-J. Shin, "Analysis of a linear piezoelectric motor driven by a single-phase signal," in *Proc. IEEE Int. Ultrason. Symp. (IUS)*, Prague, Czech Republic, Jul. 2013, pp. 481–484.

[11] C. S. Zhao, *Ultrasonic Motors: Technologies and Applications*. Berlin, Germany: Springer, 2011, pp. 15–65.

[12] B. Koc, S. Cagatay, and K. Uchino, "A piezoelectric motor using two orthogonal bending modes of a hollow cylinder," *IEEE Trans. Ultrason., Ferroelectr., Freq. Control*, vol. 49, no. 4, pp. 495–500, Apr. 2002, doi: 10.1109/58.996568.

[13] S. Cagatay, B. Koc, and K. Uchino, "A 1.6-mm, metal tube ultrasonic motor," *IEEE Trans. Ultrason., Ferroelectr.,Freq. Control*, vol. 50, no. 7, pp. 782–786, Jul. 2003, doi: 10.1109/TUFFC.2003.1214498.

[14] S. Cagatay, B. Koc, P. Moses, and K. Uchino, "A piezoelectric micromotor with a stator of Φ=1.6 mm and l=4 mm using bulk PZT," *Jpn. J. Appl. Phys.*, vol. 43, no. 4A, pp. 1429–1433, Apr. 2004, doi: 10.1143/JJAP.43.1429.
[15] K. Uchino, S. Cagatay, B. Koc, S. Dong, P. Bouchilloux, and M. Strauss, "Micro piezoelectric ultrasonic motors," *J. Electroceram.*, vol. 13, nos. 1–3, pp. 393–401, Jul. 2004, doi: 10.1007/s10832-004-5131-x.
[16] D. An, M. Yang, X. Zhuang, T. Yang, F. Meng, and Z. Dong, "Dual traveling wave rotary ultrasonic motor with single active vibrator," *Appl. Phys. Lett.*, vol. 110, no. 14, Apr. 2017, Art. no. 143507, doi: 10.1063/1.4979699.
[17] G. Wang, W. Xu, S. Gao, B. Yang, and G. Lu, "An energy harvesting type ultrasonic motor," *Ultrasonics*, vol. 75, pp. 22–27, Mar. 2017, doi: 10.1016/j.ultras.2016.11.007.
[18] T. Mashimo, "Study on micro ultrasonic motor using a preload mechanism," in *Proc. IEEE Int. Ultrason. Symp. (IUS)*, Taipei, Taiwan, Oct. 2015, pp. 1–4.
[19] S. Izuhara and T. Mashimo, "Design and evaluation of a micro linear ultrasonic motor," *Sens. Actuators A, Phys.*, vol. 118, pp. 13–16, Aug. 2018, doi: 10.1016/j.sna.2018.05.022.
[20] C. Lu, T. Xie, T. Zhou, and Y. Chen, "Study of a new type linear ultrasonic motor with double-driving feet," *Ultrasonics*, vol. 44, pp. e585–e589, Dec. 2006, doi: 10.1016/j.ultras.2006.05.191.
[21] Y. Li, Q. X. Yang, and Z. Yan, "Analysis on effective range of wireless power transfer and its impact factors," *Trans. China Electrotech. Soc.*, vol. 28, pp. 106–112, Jan. 2013.
[22] S. Park and S. He, "Standing wave brass-PZT square tubular ultrasonic motor," *Ultrasonics*, vol. 52, no. 7, pp. 880–889, Sep. 2012, doi: 10.1016/j.ultras.2012.02.010.
[23] T. Morita, M. Kurosawa, and T. Higuchi, "An ultrasonic micromotor using a bending cylindrical transducer based on PZT thin film," *Sens. Actuators A, Phys.*, vol. 50, nos. 1–2, pp. 75–80, Aug. 1995, doi: 10.1016/0924-4247(96)80087-2.
[24] K. Nakamura, M. Kurosawa, H. Kurebayashi, and S. Ueha, "An estimation of load characteristics of an ultrasonic motor by measuring transient responses," *IEEE Trans. Ultrason., Ferroelectr., Freq. Control*, vol. 38, no. 5, pp. 481–485, Sep. 1991, doi: 10.1109/58.84293.
[25] T. Mashimo, "Micro ultrasonic motor using a one cubic millimeter stator," *Sens. Actuators A, Phys.*, vol. 213, pp. 102–107, Jul. 2014, doi: 10.1016/j.sna.2014.03.018.

CHONG LI was born in Henan, China, in 1989. She received the Ph.D. degree in instrument science and technology from Shanghai Jiao Tong University, Shanghai, China, in 2017. Since 2017, she has been with Henan Normal University. Her research interest includes piezoelectric motors and their applications.

CUNYUE LU received the Ph.D. degree from the School of Mechanical and Electrical Engineering, Nanjing University of Aeronautics and Astronautics, Nanjing, China, in 2004. He is currently with Shanghai Jiao Tong University. His current research interests include piezoelectric micro motor and advanced actuator and their applications.